Measurement of sub-picoampere direct currents with uncertainties below ten attoamperes

C. Krause,[1,a)] D. Drung,[2,b)] and H. Scherer[1]
[1]*Physikalisch-Technische Bundesanstalt (PTB), Bundesallee 100, 38116 Braunschweig, Germany*
[2]*Physikalisch-Technische Bundesanstalt (PTB), Abbestraße 2-12, 10587 Berlin, Germany*

(Received 16 December 2016; accepted 26 January 2017; published online 16 February 2017)

A new type of the ultrastable low-noise current amplifier (ULCA) is presented. It involves thick-film resistors to achieve a high feedback resistance of 185 GΩ at the input amplifier. An improved noise level of 0.4 fA/$\sqrt{\text{Hz}}$ with a 1/f corner of about 30 μHz and an effective input bias current well below 100 aA are demonstrated. For small direct currents, measurement uncertainties below 10 aA are achievable even without current reversal or on/off switching. Above about 1 pA, the stability of the ULCA's resistor network limits the relative measurement uncertainty to about 10 parts per million. The new setup is used to characterize and optimize the noise in the wiring installed on a dilution refrigerator for current measurements on single-electron transport pumps. In a test configuration connected to the wiring in a pulse tube refrigerator, a total noise floor of 0.44 fA/$\sqrt{\text{Hz}}$ was achieved including the contributions of amplifier and cryogenic wiring. [http://dx.doi.org/10.1063/1.4975826]

I. INTRODUCTION

The interest in accurate direct current (dc) measurements below 1 nA becomes increasingly significant. In addition to research on electrical nanostructures such as single-electron transport (SET) devices there is also need in dosimetry, environmental technology, and modern semiconductor industry.[1] Typically, a small direct current is measured by passing it through a resistor integrated into the feedback path of an operation amplifier.[2] The resistance should be chosen as high as possible to minimize the thermal noise contribution. Practical values for the sub-picoampere range are around 1 TΩ, resulting in instruments with noise levels down to about 0.2 fA/$\sqrt{\text{Hz}}$.[3–7] Alternatively, a capacitor may be charged by the current to be measured in order to avoid the contribution of thermal noise in the resistor. In both cases the accuracy is limited, either by the stability of the high-value resistor or by the frequency dependence of the capacitance which causes an uncertainty contribution in the calibration of about 10 parts per million (ppm) at best.[8,9]

Recently, a novel amplifier was developed to enable traceable small-current measurement and generation with uncertainties down to 0.1 ppm.[9–11] This ultrastable low-noise current amplifier (ULCA) is designed as a two-stage transresistance amplifier (current-to-voltage converter) in order to obtain highest accuracy. The ULCA's first stage provides current amplification with a gain of $G_I = 1000$ by means of a complex resistor network, basically representing a matched resistor pair of $R = 3$ GΩ and $R/G_I = 3$ MΩ. The second stage performs the current-to-voltage conversion with a highly stable resistor $R_{IV} = 1$ MΩ. This results in a transresistance of $A_{\text{TR}} = \partial V_{\text{OUT}}/\partial I_{\text{S}} = G_I R_{IV} = 1$ GΩ, where V_{OUT} is the output voltage and I_{S} the input current. The ULCA's current noise floor of 2.4 fA/$\sqrt{\text{Hz}}$ is dominated by thermal noise in the 3 GΩ resistor. The 1/f noise, which becomes noticeable below about 1 mHz, mainly originates from the input amplifier. The effective input bias current (i.e., the apparent signal at the output if no current is passed into the input) is typically within ±30 fA.[12]

Usually, in high-accuracy dc measurements the input signal is modulated (i.e., periodically reversed or switched on/off) in order to suppress low-frequency excess noise and drift. The ULCA presented in Ref. 10 is well suited for measurements with repetition frequencies f_{R} (i.e., number of plus/minus or on/off cycles per second) down to about 1 mHz. However, for some applications current reversal is not possible, and on/off switching of the current compared to current reversal doubles the uncertainty at given measurement time.[10] Furthermore, at very small currents, the 2.4 fA/$\sqrt{\text{Hz}}$ noise level increases the overall uncertainty and results in long measurement times if high accuracy is needed.

In this paper, we present results obtained with a new ULCA type that is tailored for sub-picoampere direct currents and is well suited for operation without current modulation.[12] Both the current noise and the effective input bias current are considerably improved compared to the ULCA with $R = 3$ GΩ. In Sec. II, the basic model for the analysis and minimization of noise and dc errors is discussed. Sections III and IV present the analysis and measurement of noise and effective input current of the new ULCA type. In Section V an example of a practical application is given: the characterization and optimization of noise in a cryogenic setup intended for current measurements on SET devices. Section VI concludes the paper.

a)Electronic mail: Christian.Krause@ptb.de
b)Electronic mail: Dietmar.Drung@ptb.de

II. MODEL FOR NOISE AND DC ERRORS

An equivalent circuit diagram for noise and dc error analysis of the ULCA is depicted in Fig. 1. The two stages involve operational amplifiers OA1 and OA2, which are multi-stage amplifiers realized with several monolithic operational amplifiers and discrete circuits. The voltage noise V_{N1} and voltage offset V_{O1} of OA1 are taken into account by a voltage source $V_1 = V_{N1} + V_{O1}$. Equivalently, the current noise I_{N1} and bias current I_{B1} are represented by $I_1 = I_{N1} + I_{B1}$. The same applies to OA2: $V_2 = V_{N2} + V_{O2}$ and $I_2 = I_{N2} + I_{B2}$, respectively. The influence of the signal source at the ULCA input is considered by a resistance R_S and a capacitance C_S. For noise and dc error analysis, the source current I_S is assumed zero.

The equivalent circuit in Fig. 1 allows the determination of the total input current noise density S_I and effective input bias current $I_{B,\,eff}$ from the characteristics of OA1 and OA2. Figure 2 shows test circuits used for the experimental evaluation of the required data. The amplifiers OA1 and OA2 are the same as used for normal operation of the ULCA, but the resistor network of OA1 and the feedback resistor R_{IV} of OA2 are disconnected and the amplifiers are rewired to obtain the required test configurations. Careful characterization of OA1 and OA2 was necessary because the parameters specified in the data sheets of the integrated circuits were partially insufficient or even incorrect.

For simplifying the data analysis, setups were applied where the output is clearly dominated by a single parameter. In the case of "voltage effects" (i.e., voltage noise and offset voltage), the operational amplifiers are wired as a high-gain voltage amplifiers as shown in Fig. 2(a). For sufficiently low resistances in the feedback path, thermal noise in the resistors and amplifier "current effects" (i.e., current noise and bias current) become negligible. The corresponding input-referred voltage is calculated from the output voltage divided by the chosen voltage gain. The resistances quoted in Fig. 2(a) are suitable for the amplifiers used in the ULCA. They result in nominal voltage gains of 2001 and 10 001 for OA1 and OA2, respectively.

The input noise and offset voltage of the data acquisition unit can also noticeably contribute to the measurement result. Therefore, the data acquisition unit was characterized separately to remove its contribution in the data

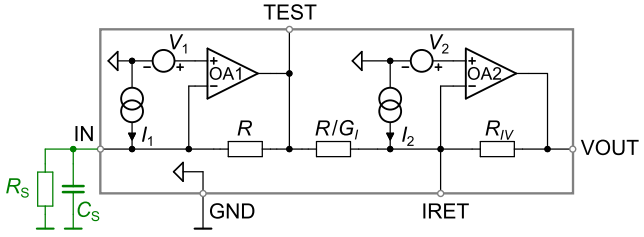

FIG. 1. Equivalent circuit for noise and dc error analysis of the ULCA. The voltage and current sources V_1, V_2, I_1, and I_2 account for the superposition of noise and offset voltage or bias current, respectively. The amplifiers OA1 and OA2 are realized by several monolithic operational amplifiers and discrete circuits. The influence of an external source at the input is represented by a resistance R_S and capacitance C_S. The latter includes the contribution of the cable connecting the source with the ULCA input.

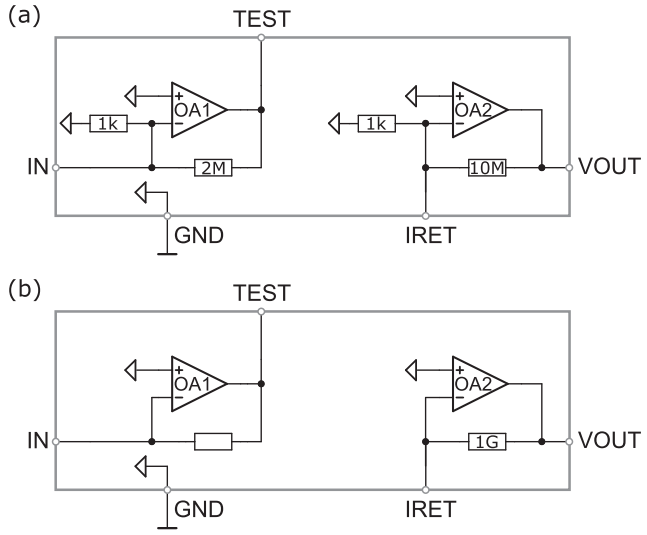

FIG. 2. Circuits for measuring the contributions of OA1 and OA2 to the total noise and effective input bias current. (a) For voltage effects from OA1 and OA2, (b) for current effect from OA2. The output signal is measured at the VOUT or TEST terminal, respectively. In (b), OA1 is not used but feedback is applied to ensure proper operating conditions.

analysis if necessary. As it will be discussed in Sec. III, amplifier OA2 involves a zero-drift amplifier in order to achieve a very low $1/f$ voltage noise. To keep the influence of the data acquisition unit low, a high gain of 10 001 was chosen for OA2. In the case of OA1 involving an amplifier with a low current noise but a relatively high voltage noise, a lower gain is sufficient. Note that the gain should not be chosen too high because otherwise the bandwidth of the amplifier might become too small for the frequency range of interest.

To measure amplifier current effects, a transresistance configuration is used as shown in Fig. 2(b). For sufficiently high feedback resistance, the contribution of voltage effects becomes negligible. As mentioned above, the use of a monolithic zero-drift amplifier at the input of OA2 leads to very low $1/f$ voltage noise and offset, but to relatively high current noise.[13] For the chosen integrated circuit, the feedback resistance of 1 GΩ quoted in Fig. 2(b) is appropriate. The 100 pF compensation capacitor of OA2 (not shown in Fig. 2(b)) affects the frequency response above about 0.1 Hz. Therefore, for high-frequency characterization, the feedback resistance was reduced to 10 MΩ and a low-noise post-amplifier with 100-fold voltage gain was applied.

In principle, current effects from OA1 can be measured similarly to those from OA2. However, the input amplifier of OA1 is selected for minimum current noise and requires a very high feedback resistance of about 1 TΩ to make the effect of thermal noise in the resistor sufficiently low. Due to stray capacitance, it is difficult to obtain the needed bandwidth. It is, hence, more convenient to measure the noise and effective bias current of the complete ULCA and to determine the current effects of OA1 by taking into account the three other contributions described above (i.e., voltage effects of OA1 and current/voltage effects of OA2). A detailed discussion of these contributions follows in Secs. III and IV.

III. AMPLIFIER NOISE

The power spectral density of the effective input current noise $S_{I,\mathrm{eff}}$ is deduced from the circuit diagram in Fig. 1, yielding

$$S_{I,\mathrm{eff}} = S_{I1} + S_{V1}\left(\left(\frac{1}{R}+\frac{1}{R_\mathrm{S}}\right)^2 + (2\pi f\, C_\mathrm{S})^2\right) + \underbrace{\frac{S_{V2}}{R^2}}_{\substack{\text{negligible for}\\ S_{V2}\ll S_{V1}}} + \underbrace{\frac{S_{V2}}{G_I R_{IV}}\left(\frac{2}{R}+\frac{1}{G_I R_{IV}}\right)+\frac{S_{I2}}{G_I^2}}_{\text{negligible for } G_I\to\infty}, \quad (1)$$

where S_{V1}, S_{V2}, S_{I1}, and S_{I2} are the power spectral densities of the voltage and current noise of OA1 and OA2, respectively. The first line in Eq. (1) describes the contribution of OA1. Obviously, the current noise S_{I1} of OA1 directly affects $S_{I,\mathrm{eff}}$. Therefore, for OA1 an input amplifier with a very good low-frequency current noise is required. Unfortunately, amplifiers tailored for minimum current noise exhibit a rather high voltage noise at low frequencies. For minimizing the voltage noise contribution, the resistances R and R_S should be as high as possible and the source capacitance C_S should be minimized. The upper limit for the resistance R depends on the target accuracy. Values between 1 GΩ and 175 GΩ were chosen for the ULCAs described in Ref. 12.

The second line in Eq. (1) shows the influence of OA2. The voltage noise contribution S_{V2}/R^2 decreases with increasing resistance R. It becomes negligible for $S_{V2} \ll S_{V1}$. Therefore, a monolithic zero-drift amplifier is used at the input of OA2. Typically, these amplifiers have excellent low-frequency voltage noise[2] which ensures that the condition $S_{V2} \ll S_{V1}$ is fulfilled in the frequency range of interest. The last terms in Eq. (1) decrease with increasing current gain G_I. They can be neglected for sufficiently high values of G_I. Due to $1/f$ noise in the amplifiers, a current gain of 1000 is not always sufficient for optimal performance in the microhertz regime. The improved ULCA presented in this paper uses G_I = 100 000, which turned out to be sufficient in all tested cases.

For finite source capacitance C_S the high-frequency current noise increases according to the term $S_{V1}(2\pi f\, C_\mathrm{S})^2$ in Eq. (1). Therefore, an operational amplifier with a voltage noise density S_{V1} as low as possible is required. The ULCA described in Ref. 10 uses an operational amplifier of type LTC6240 from Linear Technology as input amplifier for OA1.[14] This amplifier configuration (hereinafter referred to as OA1-B) has a low current noise and acceptable voltage noise between about 1 mHz and 10 Hz. Recently, the operational amplifier ADA4530-1 was introduced by Analog Devices.[15] Using this device for the ULCA (configuration OA1-A) results in a substantially reduced input bias current, but a higher voltage noise in comparison to OA1-B.

Figure 3 depicts the measured voltage noise levels of both OA1 variants along with the voltage and current noise of OA2. In the investigated frequency range covering six decades, the voltage noise density $S_{V1\text{-A}}$ of OA1-A is approximately proportional to $1/f$. The noise density $S_{V1\text{-B}}$ of OA1-B scales slightly stronger with frequency, and an additional strong rise

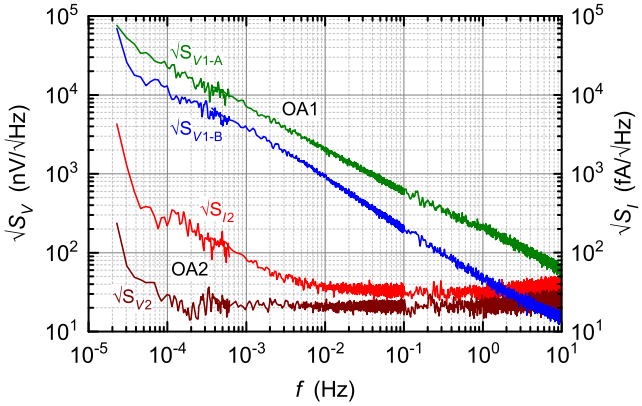

FIG. 3. Noise levels of the ULCA amplifier stages OA1 and OA2 measured with the test circuits in Fig. 2. The left scale applies to the voltage noise levels $\sqrt{S_{V1\text{-A}}}$, $\sqrt{S_{V1\text{-B}}}$ and $\sqrt{S_{V2}}$, the right scale to the current noise $\sqrt{S_{I2}}$.

occurs below about 30 μHz which is caused by temperature fluctuations in the laboratory (typically 1 K difference between day and night). For OA1-B, a temperature coefficient of −1 μV/K was estimated from the effect of the temperature fluctuations on the offset voltage, but for OA1-A no clear temperature dependence was found within its noise level. The current noise spectrum of OA2 was corrected for the thermal noise contribution of the feedback resistor. Optimized filters at the input and output of the monolithic zero-drift amplifier at the input stage of OA2 (AD8628 from Analog Devices[16]) minimize the effect of switching spikes and reduce the bias current to typically within ±2 pA. The estimated temperature coefficient of the bias current was −0.07 pA/K, but no clear correlation between the offset voltage and the environmental temperature was observed.

For sub-picoampere measurements, a new input resistor network was developed having a very high current gain of 100 000. The high-ohmic part of this network consists of 175 thick-film chip resistors (size 1206) connected in series, each with a nominal value of 1 GΩ. Combining this network with OA1-A yields the "low-bias ULCA" that features the lowest input bias current of all ULCA variants described in Ref. 12. The 1 GΩ resistors turned out to have a typical value of 1.06 GΩ which results from the voltage dependence of resistance (the parts are tested by the manufacturer at 1000 V but are operated at <1 V). Therefore, the measured R = 185 GΩ exceeds the nominal value of 175 GΩ by about 6%. For the setup with OA1-B, a prototype network was used that was equipped with a different type of resistor yielding a slightly higher resistance R = 198 GΩ.

Figure 4 shows the total noise and voltage noise contributions of OA1 in the frequency range between 10 μHz and 10 Hz. The voltage noise contributions were deduced from the voltage noise densities S_{V1} depicted in Fig. 3. Different values for C_S are assumed in Fig. 4 in order to cover the relevant range of source capacitance. At high frequencies the voltage noise contribution increases with the source capacitance C_S. The highest value C_S = 640 pF is equal to the total capacitance of the cable combination in Sec. V. The total noise with this cable combination (corresponding to the gray-colored curves in Fig. 4) increases at high frequencies compared to the case without cable. This increase is caused by the voltage

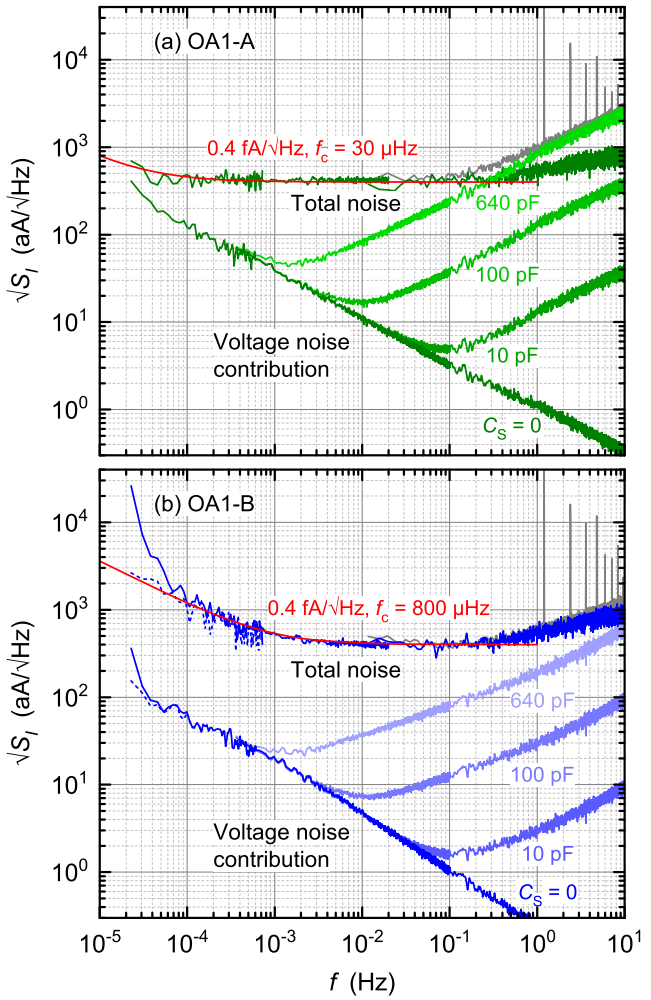

FIG. 4. Total noise of the ULCA and voltage noise contributions obtained for different operational amplifiers OA1 and source capacitances C_S. (a) OA1-A optimized for low frequencies and (b) OA1-B intended for high frequencies. The voltage noise contribution for various values of C_S was determined from the measured noise density S_{V1} by applying Eq. (1). For comparison, the total noise with a cable at the ULCA input having 640 pF capacitance is depicted as gray lines (see Sec. V for details). In (b), dotted curves show the noise corrected for the temperature dependence of +0.4 fA/K (total noise) and −1 µV/K (voltage noise contribution), respectively. The red curves are calculated assuming white and 1/f noise according to Eq. (2).

noise contribution. Note that the high-frequency increase of the total noise without cable connected to the input is presumably caused by stray capacitance in the resistor network. The red curve for the total noise of OA1-A and OA1-B takes into account white and 1/f noise according to

$$S = S_w \left(1 + \frac{f_c}{f}\right) . \tag{2}$$

The total spectral density S is approximated by a superposition of the white noise density S_w and the 1/f noise contribution.[2] The 1/f corner f_c defines the frequency at which both contributions are equal. Using the equations in Ref. 17, the Allan variance σ^2 for the superposition of white and 1/f noise is found to be

$$\sigma^2 = S_w \cdot \left(\frac{1}{2\tau} + 2\ln(2) \cdot f_c\right) , \tag{3}$$

where τ is the sampling time. The white noise levels were determined from the measured spectra (total noise in Fig. 4)

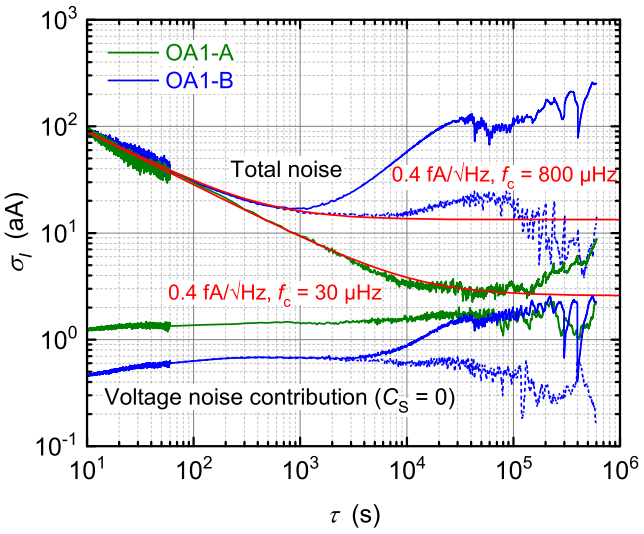

FIG. 5. Allan deviation of the measured time data used for the noise spectra in Fig. 4. The red curves are calculated with Eq. (3). The dotted curves show the Allan deviation of OA1-B corrected for the temperature dependence of +0.4 fA/K (total noise) and −1 µV/K (voltage noise contribution).

in a small region around 0.1 Hz, and the 1/f noise corners f_c were adjusted with the help of Eqs. (2) and (3) to obtain good agreement between the red curves and the measurement data in Figs. 4 and 5.

Figure 5 shows the Allan deviation σ_I for the total noise and the voltage noise contribution with zero source capacitance ($C_S = 0$) in the time domain of 10 s – 10^6 s. The same raw data were used as for the noise spectra in Fig. 4. For both amplifier variants the total white noise is about 0.4 fA/√Hz, but the 1/f corner frequencies differ substantially. OA1-A shows an exceptionally low value $f_c = 30$ µHz which means that the noise is white even for sampling times exceeding 1 h. For the setup with OA1-B, the Allan deviation strongly degrades at long sampling times due to temperature effects. The experimentally observed temperature coefficients are +0.4 fA/K for the total noise and −1 µV/K for the voltage noise contribution. By correcting the temperature dependence, the Allan deviation is significantly reduced, corresponding to increased accuracy at long sampling times. The temperature-corrected voltage noise contribution of OA1-B is even lower than for OA1-A, but the resulting 1/f corner frequency of the total noise of 800 µHz is still substantially higher than for the setup with OA1-A that shows no noticeable temperature dependence.

IV. EFFECTIVE INPUT BIAS CURRENT

The effective input bias $I_{B,eff}$ is the apparent input current displayed at the output if no source is connected to the amplifier. It is defined as V_{OUT}/A_{TR}, where V_{OUT} is the output voltage with open input and $A_{TR} = G_I R_{IV}$. Using the circuit diagram in Fig. 1, the contributions of OA1 and OA2 are found to be

$$I_{B,eff} = \underbrace{I_{B1} - V_{O1}\left(\frac{1}{R} + \frac{1}{R_S}\right)}_{OA1} - \underbrace{\frac{I_{B2}}{G_I} + V_{O2}\left(\frac{1}{G_I R_{IV}} + \frac{1}{R}\right)}_{OA2} . \tag{4}$$

Sorting the terms by resistances leads to

$$I_{\mathrm{B,eff}} = I_{\mathrm{B1}} - \frac{V_{\mathrm{O1}}}{R_{\mathrm{S}}} + \frac{V_{\mathrm{O2}} - V_{\mathrm{O1}}}{R} + \underbrace{\frac{1}{G_I}\left(\frac{V_{\mathrm{O2}}}{R_{IV}} - I_{\mathrm{B2}}\right)}_{\text{negligible for } G_I \to \infty}. \quad (5)$$

It is obvious that I_{B1} directly affects $I_{\mathrm{B,eff}}$. The bias current contribution resulting from the voltage offset V_{O1} of OA1 depends on both the source resistance R_{S} and the feedback resistance R. As the ULCA involves a monolithic zero-drift amplifier at the input of OA2, a very low offset voltage V_{O2} is achieved, which makes the resulting bias current contribution negligible. Furthermore, for high values of G_I the last term of Eq. (5) can also be neglected.

Figure 6 shows $I_{\mathrm{B,\,eff}}$ for OA1-A and OA1-B taken over a period of 14 days. The measurement was done with a sampling rate of 16 points per second. Each measurement point in Fig. 6 is taken over an integration time of $\tau = 1$ h. The laboratory was not temperature-stabilized, resulting in strong temperature variations of nearly 3 K peak-to-peak, see Fig. 6(a). Temperature variations corresponding to day/night cycles are clearly visible. For OA1-B the temperature fluctuations lead to $I_{\mathrm{B,\,eff}}$ fluctuations of about 1.1 fA peak-to-peak with a temperature coefficient of +0.4 fA/K. In the case of OA1-A the mean value is about −20 aA and no clear temperature dependence is visible.

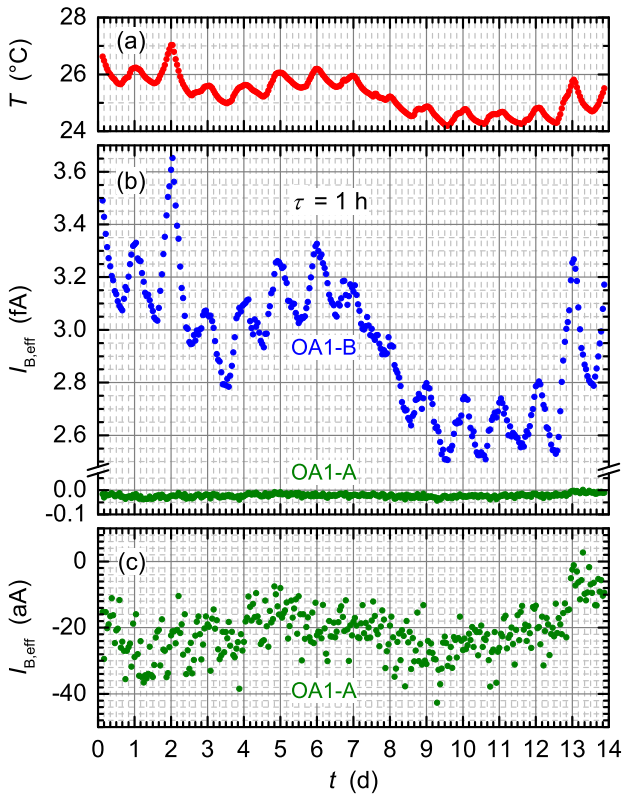

FIG. 6. (a) Temperature T and (b) effective input bias current $I_{\mathrm{B,eff}}$ for the ULCAs with OA1-A and OA1-B measured over a period of two weeks. Temperature oscillations corresponding to day/night cycles are clearly visible. In (c) a magnification from the result of OA1-A is depicted. Each data point shows the mean value over a sampling time $\tau = 1$ h.

All results presented so far were obtained with zero input current. To determine the performance in a real dc measurement, two low-bias ULCAs were combined. One of them was set into source mode for current generation, while the other was set into amplifier mode for current measurement.[10] The output voltages of the two ULCAs were measured with Keysight 3458A voltmeters at an effective sampling rate of 47 samples per second (1 power line cycle of integration time per point and auto-zero performed every 2 s). The generated current I_{SRC} and the measured current I_{AMP} were obtained by dividing the respective ULCA output voltage by the corresponding transresistance. The uncertainty of the difference $\Delta I = I_{\mathrm{AMP}} - I_{\mathrm{SRC}}$ represents the total measurement uncertainty. If the uncertainty contributions of both ULCAs are equal, the total uncertainty is a factor of $\sqrt{2}$ higher than for the individual ULCAs. The temperature was monitored but the effect of temperature fluctuations (typically 1 K peak-to-peak during a measurement) was not corrected for to get the performance in harsh laboratory conditions.

The measurements were done both without and with current reversal at two levels (1 fA and 1 pA). Figure 7(a) shows the results at low level. Here, the total uncertainty is always dominated by noise and drift because the fluctuations of the

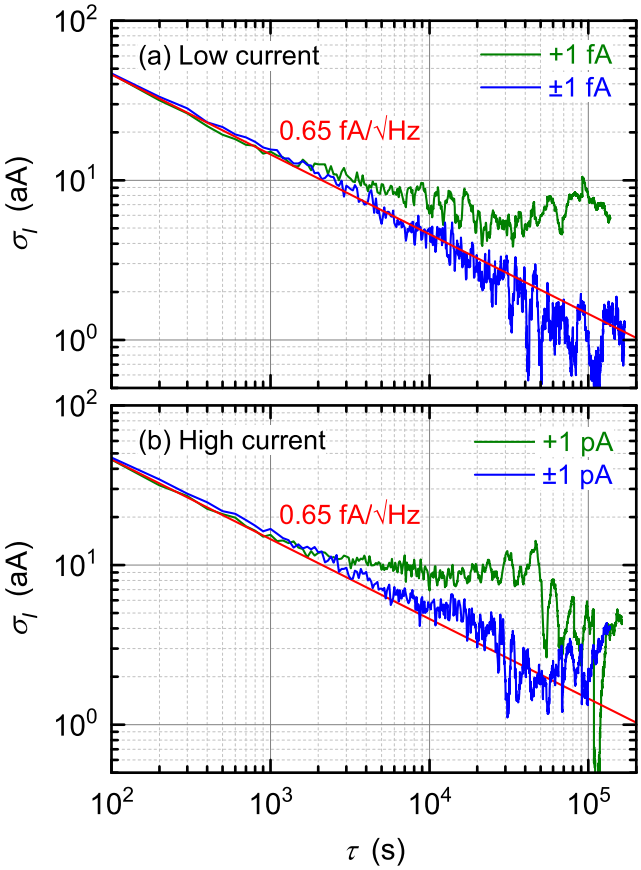

FIG. 7. Allan deviation σ_I of the difference $\Delta I = I_{\mathrm{AMP}} - I_{\mathrm{SRC}}$ between the currents generated by an ULCA in source mode and measured by another ULCA operated in amplifier mode. (a) Low current level of 1 fA and ±1 fA, and (b) high current level of 1 pA and ±1 pA. In the cases of bipolar current, the current were reversed every 50 s and, the first 5 s after each reversal was disregarded. The output voltages of the ULCAs were measured with 3458A voltmeters. The red lines show white noise calculated with Eq. (3).

ULCA transresistance (rms value typically well below 10 ppm) cause a negligible uncertainty contribution of $\ll 1$ aA. Without current reversal, the Allan deviation reaches a minimum of about 6 aA at $\tau \approx 8$ h, limited by $1/f$ noise and bias current stability. In contrast, with current reversal, the noise is white in the full range of τ as expected.[9] A very low uncertainty of 2 aA (corresponding to 1.4 aA for the individual ULCA) is achieved for an integration time $\tau \approx 15$ h. Effective white noise levels of $\sqrt{2} \cdot 0.4\ \mathrm{fA}/\sqrt{\mathrm{Hz}} = 0.57\ \mathrm{fA}/\sqrt{\mathrm{Hz}}$ and $(0.57/\sqrt{0.9})\ \mathrm{fA}/\sqrt{\mathrm{Hz}} = 0.6\ \mathrm{fA}/\sqrt{\mathrm{Hz}}$ are expected for the cases without and with current reversal (the effective noise with current reversal is higher because 10% of the sampled data are disregarded to suppress settling effects).[10] The experimental value is slightly higher, $0.65\ \mathrm{fA}/\sqrt{\mathrm{Hz}}$, presumably caused by aliasing effects in the 3458A voltmeters.[11] The noise contribution of the 1 m long low-noise cable connecting the two ULCAs was found to be negligible.

At higher current levels of 1 pA (without current reversal) and ±1 pA (with current reversal), the low-frequency fluctuations of the ULCA transresistances become noticeable, as depicted in Fig. 7(b). Therefore, at long integration times τ the measurement uncertainty is slightly degraded compared to the low current case. The achieved uncertainty of about 10 aA at 1 pA corresponds to a relative uncertainty of 10 ppm. With current reversal, uncertainties well below 10 aA or 10 ppm are achievable. Note that the presented measurements include noise and transresistance fluctuations/drift only. Systematic uncertainties caused by the linearity of the resistor networks and the finite calibration accuracy are not considered here. They are estimated to typically remain below 10 ppm.[12]

V. CABLE NOISE MEASUREMENTS

Quantum current sources based on single electron transport (SET) devices are candidates for realizing the ampere according to its future definition in the revised SI.[18–22] They are typically operated in cryogenic refrigerators at millikelvin temperatures and are able to accurately source currents of the order of 100 pA. The SET-generated current is transferred to current amplification and data acquisition instrumentation outside the refrigerator via low-noise cables. This imposes highest demands on the quality of the cryogenic wiring, since cables typically exhibit parasitic effects such as microphonic, piezo-, and triboelectric effects. Triggered by mechanical vibrations, these can cause excess current noise.[7]

To investigate possible excess noise, a test configuration involving the amplifiers described in Secs. II–IV wasimplemented. The measurements were performed in an Oxford Instruments DR200 dilution refrigerator with a pulse tube for pre-cooling and condensing the ^{3}He and ^{4}He mixture. The wiring was composed of three different cable segments as shown in Fig. 8. For the connection between the amplifier and the output of the refrigerator a room temperature low-noise coaxial cable of 1 m length was used. The insulator material of this cable is polyethylene (PE) with a conducting polyvinyl chloride (PVC) layer. A conductive layer between outer conductor and insulator is typically included in low-noise cables

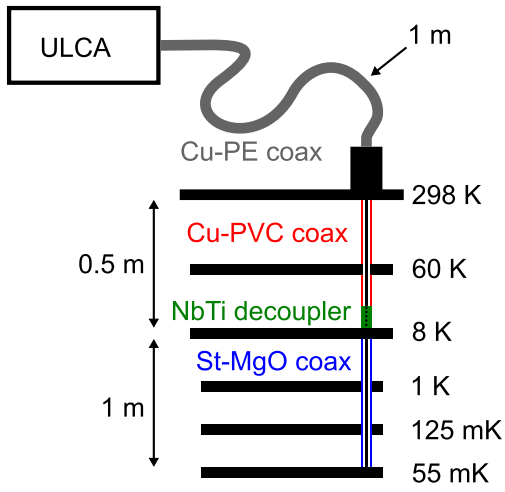

FIG. 8. Wiring concept developed for the measurement of currents generated by SET devices.

for room temperature applications to reduce the influence of parasitic effects.[23]

Inside the refrigerator, a Cu-PVC coaxial cable (length 0.5 m) was installed between 298 K and 8 K. The outer conductor was thermally anchored at the 60 K and 8 K stages. The inner conductor was thermally decoupled at 8 K with a short niobium-titanium wire. From 8 K down to 55 mK a semi rigid steel cable (Thermocoax, length 1 m) with a cover cap at the end was used. This cable involves magnesium oxide (MgO) powder as an insulator. The cables were electrically connected by SMA and MCX connectors. In order to reduce possible mechanical vibrations, the cables inside the refrigerator were mechanically fixed by cable ties and bare copper wires. Cable properties according to their manufacturer specifications are listed in Table I.

Noise measurements were performed in the frequency range from 10 Hz down to 10 μHz. The high-frequency spectra were measured using the ULCA involving OA1-B and the low-frequency spectra using the low-bias ULCA involving OA1-A. An NI-6211 card was applied for data acquisition showing an offset of 50 μV that was corrected for in the data

TABLE I. Properties of the three cables used in the cryogenic setup depicted in Fig. 8.

Name	Cu-PE coax	Cu-PVC coax	St-MgO coax
Cable type	BEDEA MXR	LEMO 280630	Thermocoax 1NcAc034
Inner conductor	Cu strand 7 × 0.15 mm	Cu strand 7 × 0.1 mm	Steel
Insulator	PE	PVC	MgO (powder)
Outer conductor	Cu braid 32 × 0.15 mm & cond. PVC	Cu wires 32 × 0.1 mm	Steel Ø = 0.35 mm
Sheath	PVC	PVC	—
Length (m)	1	0.5	1
Capacitance (pF)	120	50	470

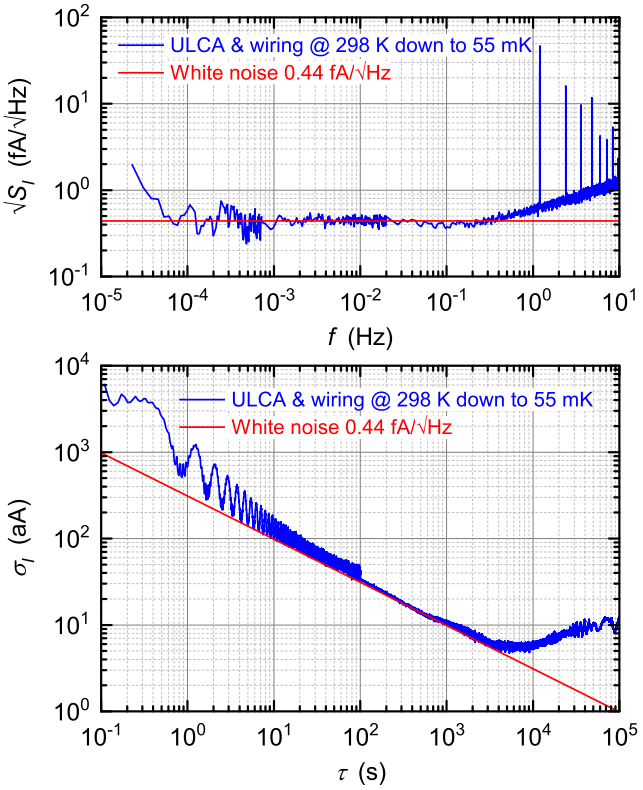

FIG. 9. Current noise and Allan deviation measured with the cryogenic setup shown in Fig. 8.

analysis. The 70 aA input bias current of the low-bias ULCA plus connected cable was separately measured with a 3458A voltmeter. Results of the noise measurements are shown in Fig. 9. At higher frequencies, the fundamental frequency and harmonics caused by the pulse tube unit are clearly visible in the current noise spectra. The total white noise of about 0.44 fA/$\sqrt{\text{Hz}}$ is dominated by the intrinsic noise of the low-bias ULCA. The Allan deviation shows a minimum of about 6 aA at $\tau \approx 2$ h and remains below 10 aA for $1/2\,\text{h} < \tau < 8$ h. Due to the very low noise level the presented cryogenic wiring should be well suited for demanding measurements on quantum current standards.

VI. CONCLUSION

A low-bias ULCA tailored for sub-picoampere currents was presented that features an input bias current well below 100 aA and a noise level of 0.4 fA/$\sqrt{\text{Hz}}$ with a remarkably low $1/f$ corner frequency of about 30 μHz. The input bias current is very stable in time and temperature, allowing sensitive dc measurements in laboratory environment without temperature stabilization. Due to the good low-frequency noise performance, a very low measurement uncertainty of 10 aA is achieved in a relatively short sampling time $\tau \approx 1/2$ h, both with and without current reversal. The presented ULCA allows the traceable measurement of small direct currents with relative uncertainties down to 10 ppm. It is expected to set new benchmarks in the small-current regime.

ACKNOWLEDGMENTS

The authors thank Michael Piepenhagen and Maximilian Luther for fabrication and assembling of printed-circuit boards and Jan-Hendrik Storm, Marco Schmidt, and Jörn Beyer for assistance in making cryogenic measurements. This work was supported in part by the Joint Research Project "e-SI-Amp" (15SIB08). This project has received funding from the European Metrology Programme for Innovation and Research (EMPIR) co-financed by the participating states and from the European Union's Horizon 2020 research and innovation programme.

[1] N.-H. Kaneko, S. Nakamura, and Y. Okazaki, "A review of the quantum current standard," Meas. Sci. Technol. **27**, 032001 (2016).
[2] P. Horowitz and W. Hill, *The Art of Electronics* (Cambridge University Press, 2015).
[3] J. Yao and J. Yoon, "Low-noise electrometer and its low-noise cryogenic probe with completely guarded sample chamber," Rev. Sci. Instrum. **71**, 1776–1780 (2000).
[4] M. Carlà, L. Lanzi, E. Pallecchi, and G. Aloisi, "Development of an ultralow current amplifier for scanning tunneling microscopy," Rev. Sci. Instrum. **75**, 497–501 (2004).
[5] Keithley, Counting electrons: How to measure currents in the attoampere range, 2005, see http://www.tek.com/sites/tek.com/files/media/document/resources/2648%20Counting%20Electrons1.pdf.
[6] Femto, Datasheet DDPCA-300, 2016, see http://www.femto.de/de/produkte/stromverstaerker/sub-femtoampere-var-verstaerkung-ddpca.html.
[7] E. Mykkänen, J. S. Lehtinen, A. Kemppinen, C. Krause, D. Drung, J. Nissilä, and A. J. Manninen, "Reducing current noise in cryogenic experiments by vacuum-insulated cables," Rev. Sci. Instrum. **87**, 105111 (2016).
[8] S. P. Giblin, G. D. Willenberg, and N. E. Fletcher, "Frequency dependence of gas-dielectric capacitors used in sub-nA reference current generators," in *Digest of 27th Conference on Precision Electromagnetic Measurements (CPEM 2010), Daejeon, Korea* (Institute of Electrical and Electronics Engineers (IEEE), 2010).
[9] D. Drung, M. Götz, E. Pesel, and H. Scherer, "Improving the traceable measurement and generation of small direct currents," IEEE Trans. Instrum. Meas. **64**, 3021–3030 (2015).
[10] D. Drung, C. Krause, U. Becker, H. Scherer, and F. J. Ahlers, "Ultrastable low-noise current amplifier: A novel device for measuring small electric currents with high accuracy," Rev. Sci. Instrum. **86**, 024703 (2015).
[11] D. Drung, C. Krause, S. P. Giblin, S. Djordjevic, F. Piquemal, O. Séron, F. Rengnez, M. Götz, E. Pesel, and H. Scherer, "Validation of the ultrastable low-noise current amplifier as travelling standard for small direct currents," Metrologia **52**, 756–763 (2015).
[12] D. Drung and C. Krause, "Ultrastable low-noise current amplifiers with extended range and improved accuracy," IEEE Trans. Instrum. Meas. **66**(6), 1 (2016).
[13] D. Drung and C. Krause, "Excess current noise in amplifiers with switched input," IEEE Trans. Instrum. Meas. **64**, 1455–1459 (2015).
[14] Linear Technology, Datasheet LTC6240, 2010, see http://www.linear.com/product/LTC6240.
[15] Analog Devices, Datasheet ADA4530-1, 2016, see http://www.analog.com/en/products/amplifiers/operational-amplifiers/ada4530-1.html.
[16] Analog Devices, Datasheet AD8628, 2014, see http://www.analog.com/en/products/amplifiers/operational-amplifiers/zero-drift-amplifiers/ad8628.html.
[17] T. Witt, "Allan variances and spectral densities for DC voltage measurements with polarity reversals," IEEE Trans. Instrum. Meas. **54**, 550–553 (2005).
[18] J. P. Pekola, O.-P. Saira, V. F. Maisi, A. Kemppinen, M. Möttönen, Y. A. Pashkin, and D. V. Averin, "Single-electron current sources: Toward a refined definition of the ampere," Rev. Mod. Phys. **85**, 1421–1472 (2013).
[19] B. Kaestner and V. Kashcheyevs, "Non-adiabatic quantized charge pumping with tunable-barrier quantum dots: A review of current progress," Rep. Prog. Phys. **78**, 103901 (2015).
[20] L. Fricke, M. Wulf, B. Kaestner, F. Hohls, P. Mirovsky, B. Mackrodt, R. Dolata, T. Weimann, K. Pierz, U. Siegner, and H. W. Schumacher, "Self-referenced single-electron quantized current source," Phys. Rev. Lett. **112**, 226803 (2014).

[21]F. Stein, D. Drung, L. Fricke, H. Scherer, F. Hohls, C. Leicht, M. Götz, C. Krause, R. Behr, E. Pesel, K. Pierz, U. Siegner, F. J. Ahlers, and H. W. Schumacher, "Validation of a quantized-current source with 0.2 ppm uncertainty," Appl. Phys. Lett. **107**, 103501 (2015).

[22]F. Stein, H. Scherer, T. Gerster, R. Behr, M. Götz, E. Pesel, C. Leicht, N. Ubbelohde, T. Weimann, K. Pierz, H. W. Schumacher, and F. Hohls, "Robustness of single-electron pumps at sub-ppm current accuracy level," Metrologia **54**, S1 (2017).

[23]C. Krause, H. Scherer, and D. Drung, "Cable noise investigations for high-accuracy measurements of small direct currents," in *Digest of 30th Conference on Precision Electromagnetic Measurements (CPEM 2016)* (Institute of Electrical and Electronics Engineers (IEEE), Ottawa, Canada, 2016).